



A decade-long hydrographic moored time series near the Drygalski Ice Tongue, Terra Nova Bay, Ross Sea

Liv Cornelissen^{1,2}, Sukeyoung Yun³, Jasmin McInerney¹, Brett Grant¹, Fiona Elliott^{1,b},
Seung-Tae Yoon^{3,a}, Christopher J. Zappa⁴, Won Sang Lee³, and Craig Stevens^{1,2}

¹Earth Sciences New Zealand, formerly National Institute of Water and Atmospheric Research,
Greta Point, Wellington 6021, New Zealand

²Department of Physics, University of Auckland, Auckland 1142, New Zealand

³Korea Polar Research Institute, Yeonsu-gu, Incheon 21990, Republic of Korea

⁴Lamont Doherty Earth Observatory, Columbia University, Palisades, NY, USA

^anow at: Kyungpook National University, Daegu, Republic of Korea

^bnow at: University of Bergen, Bergen, Norway

Correspondence: Liv Cornelissen (liv.cornelissen@otago.ac.nz)

Received: 3 September 2025 – Discussion started: 17 September 2025

Revised: 6 March 2026 – Accepted: 18 March 2026 – Published: 10 June 2026

Abstract. In this paper we describe a decade-long timeseries of hydrographic mooring observations adjacent to the Drygalski Ice Tongue in southern Terra Nova Bay, Antarctica. Unique aspects of the data are that (i) the instruments were placed very close to the Ice Tongue which has significant influence on the region's ocean and sea ice, and (ii) the upper sensors were positioned relatively close (< 100 m) to the ocean surface compared to typical Antarctic moorings. Starting in December 2014, the mooring array included three locations – the Drygalski Basin, the edge of the Cray Bank and, on the southern side of the ice tongue, in Geikie Inlet. The instruments measure temperature, salinity, pressure, and current velocity. The “DITx” mooring locations were chosen in order to support questions regarding the influence of the Drygalski Ice Tongue on regional ocean processes. The observations are relevant to water mass formation, glaciology and ice melt, sea ice production and decay, ice shelf cavity processes – as well as regional marine ecosystem processes. The data from the instruments show the seasonal cycle along with interannual variability, as well as a range of singular events. All data can be downloaded from the SEANOE database (<https://doi.org/10.17882/102640>; Cornelissen et al., 2025).

1 Introduction

1.1 The Drygalski Ice Tongue and Terra Nova Bay

The Drygalski Ice Tongue is presently the largest ice tongue in Antarctica and it forms the southern boundary of Terra Nova Bay (TNB), Western Ross Sea, Antarctica. It is the floating extension of the David Glacier and plays a crucial role in maintaining the Terra Nova Bay polynya by limiting northward-flowing of sea ice along the Victoria Land Coast (Gomez-Fell et al., 2023). The free floating part of the ice tongue extends ~ 80 – 90 km into the Ross Sea, with a width of ~ 20 km (Stevens et al., 2017) as shown in Fig. 1, which makes it presently Antarctica's largest free-floating

glacier (Frezzotti and Mabin, 1994). At the grounding line the glacier is more than 1900 m thick (Indrigo et al., 2021; Bianchi et al., 2001). The glacier then thins to the extent that the tip, located above the edge of the Cray Bank in a water depth of 600–700, is ~ 200 m thick (Indrigo et al., 2021). Despite the blocking effect of the ice tongue on sea ice and surface water masses, Stevens et al. (2024) determined that there is exchange and advection of water masses in the ocean below the floating ice.

Terra Nova Bay is bounded to the south by the Drygalski Ice Tongue and to the west by the Nansen Ice Shelf, which is fed by the Priestly and Reeves Glacier. A key bathymetric feature, the Drygalski Basin, extends north east into the Dry-

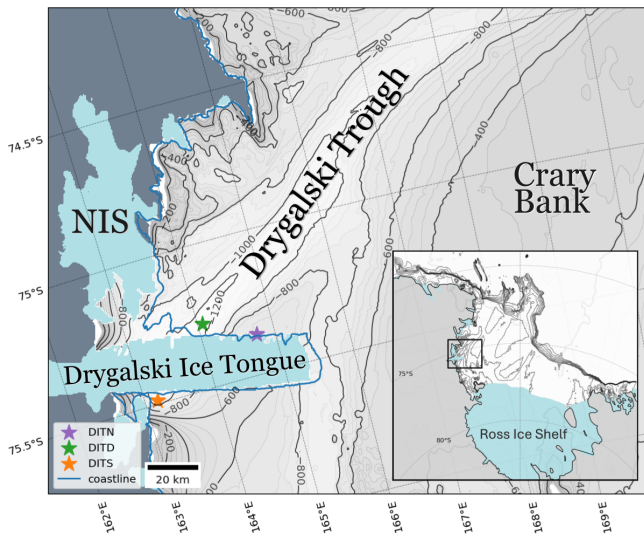


Figure 1. Terra Nova Bay (TNB) is located in the western Ross Sea. The Nansen Ice Shelf (NIS) bounds the bay in the west, the Drygalski Ice Tongue bounds the bay on the southern side and the deepest part of Terra Nova Bay is the Drygalski Basin. The eastern boundary of the Drygalski trough is the Crary bank. The DITx mooring locations are marked on the bathymetry of Terra Nova Bay with a Star, the grey contours are the bathymetry at 50 m intervals with solid lines on 200 m intervals using BedMachine3 (Morlighem et al., 2020). The light-blue area represents the floating sea ice, the Nansen Ice shelf and Drygalski Ice Tongue. The grey represents the land. The blue line represents the coastline from 2014 (Haran et al., 2018). DITN mooring was first deployed in December 2014, DITD was first deployed in February 2017 and DITS was deployed from February 2017 until January 2020.

galski Trough and is believed to be the primary export pathway for High Salinity Shelf Water (HSSW). Along the eastern boundary, the Victoria Land Coast Current carries water and sea ice northward from McMurdo Sound (Stevens et al., 2017). This flow has been inferred from satellite sea ice drift and surface drifters (Otago Sea Ice Monitoring, 2026) and is reproduced in ocean circulation models such as GLO-RYS and P-SKRIPS (Malyarenko et al., 2023; Gossart et al., 2025), though its vertical structure and depth extent remain poorly constrained by direct observations between McMurdo Sound and Terra Nova Bay. This current could also bring water masses into Terra Nova Bay below the Drygalski Ice Tongue or along the Drygalski Ice Tongue as replenishing the HSSW outflow.

The polynya that occasionally forms in Terra Nova Bay is relatively small in extent when compared to the nearby Ross Sea polynya (Morales Maqueda et al., 2004) but plays an important role in the global climate system. Between autumn and spring, strong katabatic winds blow off the Nansen Ice Shelf, pushing the sea ice off the coast and enabling heat loss from the relatively warm ocean to the cold atmosphere, and producing sea ice and HSSW. Despite its small size in global

terms, Terra Nova Bay accounts for approximately 3%–4% of Antarctic sea ice production (Tamura et al., 2016), and up to 10% of Antarctic Bottom Water (AABW). Sea ice makes ship-based observations very difficult from late autumn when these important water masses are formed and HSSW is an important water mass that contributes to basal melting of floating glaciers and ice shelves (Nicholls, 1997). Hydrographic moorings, that observe water masses throughout the year are therefore an essential tool to study the oceanographic processes in Terra Nova Bay polynya. While moorings in the central Terra Nova Bay have provided a long term perspective of water mass transformation (MORSea, 2009; Castagno et al., 2019), the strong influence of the Drygalski Ice Tongue on the region provided motivation for a mooring array (hereinafter called the “DITx” array) focused around the Drygalski Ice Tongue.

1.2 Processes that interact with the Drygalski Ice Tongue

One of the key processes influencing the region are the occasional katabatic-driven polynya events. In such conditions, the fast, cold katabatic winds drive sea ice formation at the ocean surface, which results in the creation of HSSW as a by-product (e.g., Yoon et al., 2020; Friedrichs et al., 2022). The brine rejection from the sea ice formation first breaks down the stratification of the water column in the polynya before HSSW starts to form. While the production of HSSW begins in late Autumn/early winter, the salinity increase does not increase until September at the bottom in the eastern side of Terra Nova Bay, where DITN is located, and in the Drygalski Basin (Yoon et al., 2020). Figure 2 shows the seasonal evolution of stratification in Terra Nova Bay, based on a summer CTD profile and Argo float observations from both summer and winter (Argo, 2000). The circulation pattern in Terra Nova Bay is described by Yoon et al. (2020), based on summer CTD observations and three hydrographic moorings between December 2014 and March 2018 and include data from the hydrographic moorings described in this paper (DITN and DITD). They observed a cyclonic circulation in the deeper part of Terra Nova Bay between 400–700 m during the summer, which advects the HSSW created close to the Nansen Ice shelf, which is considered to be the primary location of HSSW production in Terra Nova Bay, towards the DITN, where the salinity increase is observed by the bottom instrument of this mooring. The salinity increases at this depth are observed between September and October, and not at the start of winter when the stratification has broken down. Rusciano et al. (2013) suggested that HSSW is advected from the Nansen Ice Shelf front towards eastern Terra Nova Bay and was confirmed in Yoon et al. (2020).

Terra Nova Bay Ice Shelf Water (TISW) is formed when HSSW interacts with basal melt waters from the Drygalski Ice Tongue and the Nansen Ice Shelf during active HSSW production. TISW is characterized by a conserved tempera-

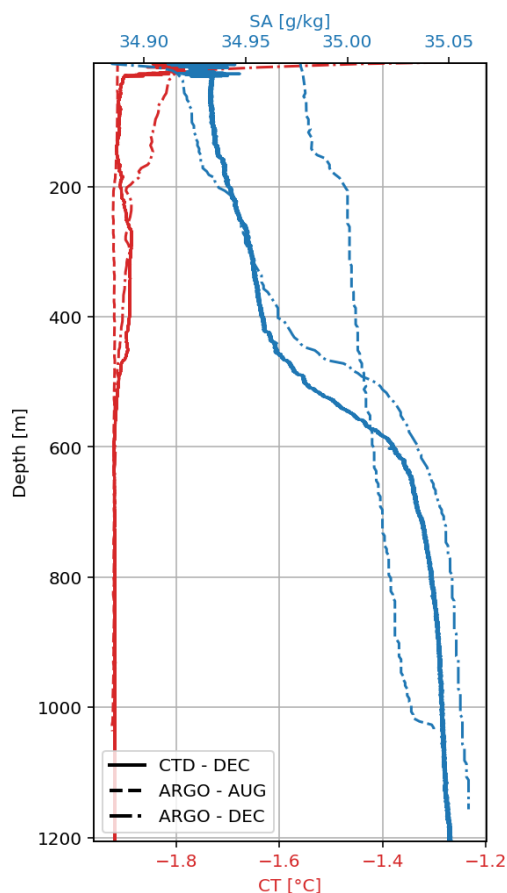


Figure 2. Vertical profiles of conservative temperature (red) and absolute salinity (blue) within Terra Nova Bay. The CTD profile from December 2022 is shown as solid lines, while ARGO float (Argo, 2000) measurements are shown for winter (dashed lines) and summer (dash-dotted lines). This comparison highlights seasonal variations in the upper water column.

ture below the surface freezing temperature around -1.94°C depending on the salinity (Yoon et al., 2020) and a density larger than 1028 kg m^{-3} (e.g., Rusciano et al., 2013; Yoon et al., 2020, their Fig. 6). The characteristics of TISW observed in summer in Yoon et al. (2020) depends on observation period and the outflow from under the Nansen Ice Shelf and is believed to advect in the same cyclonic circulation as HSSW towards the eastern Terra Nova Bay. TISW is also observed in the eastern Terra Nova Bay close to Drygalski Ice Tongue by DITN; further study needs to investigate if this TISW is formed under the Nansen Ice Shelf and advected or is formed when HSSW interacts with basal melt waters from the Drygalski Ice Tongue itself. Antarctic Surface Water (AASW) can be found at the subsurface and originates from the melting of the sea ice. It is a fresh and relatively warm ($> -1.7^{\circ}\text{C}$, Friedrichs et al., 2022) water mass as it warms through solar radiation during Summer (Rusciano et al., 2013). As its density is much lower than the water masses formed during winter, it contributes to the restratification of

the water column during the summer months. The stratification driven by the AASW and the breakdown of the stratification driven by the HSSW formation is shown in Fig. 2. The CTD profiles are also used for instrument calibration, as described in Sect. “Quality control” and Fig. 2.

1.3 Monitoring the water masses around the Drygalski Ice Tongue

The DITx hydrographic moorings distributed around the Drygalski Ice Tongue have been maintained since December 2014 in order to monitor the water mass properties and currents close to the ice tongue. Three moorings were deployed over different time frames, located around the Drygalski Ice Tongue as shown in Fig. 1. DITN is a long mooring deployed on the northern side of the Drygalski Ice Tongue from December 2014 to the present. It includes instruments near the seafloor, mid-water column, and subsurface, with the shallowest instrument at 75 m depth. The upper instruments are at risk of collisions from icebergs calving off the Drygalski Ice Tongue, which are frequent in the area and can extend to great depths. Despite this risk, the setup is unique and essential for studying subsurface processes. Its proximity to the ice tongue and near-surface coverage make it particularly well suited to investigate subsurface circulation and the influence of meltwater. DITD, a short mooring deployed in February 2017 and still active, is located in the deepest part of the Drygalski Basin. It captures the densest HSSW observed in the area, offering a valuable reference point for comparing water mass properties with other locations. DITS was a long mooring positioned south of the Drygalski Ice Tongue in Geikie Inlet and was maintained from February 2017 until January 2020. This paper presents a comprehensive overview of the decadal dataset collected by the DITx array. The data are freely available via SEANOE in netCDF format, organized by mooring, instrument type, and deployment year (Cornelissen et al., 2025). Tables 3, 4, and 5 summarize the mooring configurations, and instrument placements are visualized in Figs. 3 and 4.

In addition to these moorings, other relevant datasets in the region include the MORSea Moorings D and L (MORSea, 2009; Castagno et al., 2019) and a Lamont-Doherty Earth Observatory (LDEO) mooring (Miller et al., 2024) located near the front of the Nansen Ice Shelf (Miller et al., 2024). Since 2013, Argo floats have also contributed valuable data to the Ross Sea, with four deployed in Terra Nova Bay during 2021, 2022, 2024, and 2025 (Argo, 2000).

2 The DITx hydrographic mooring time series

Three hydrographic moorings have been deployed from December 2014 in the Terra Nova Bay polynya equipped with CTD instruments (Sea-Bird Scientific, 2026a), thermistors (Sea-Bird Scientific, 2026c) and current meters (RCM9, Xylem Inc., 2026, until 2017 and Aquadopp, Nortek, 2026,

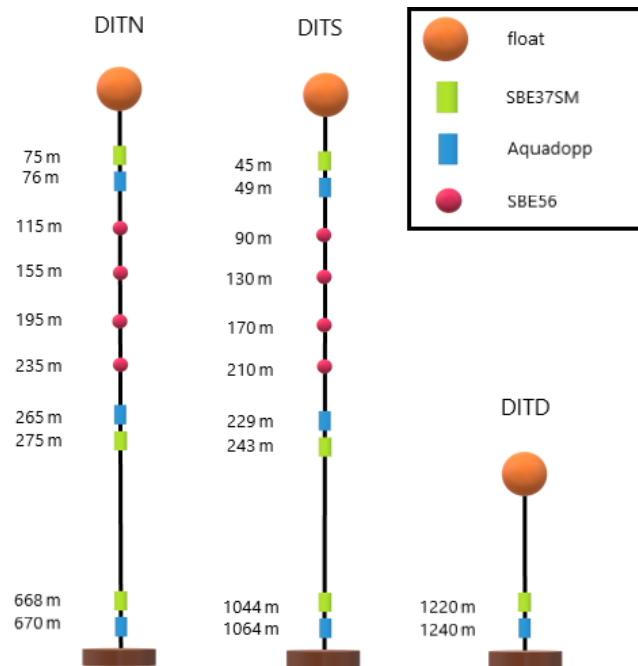


Figure 3. A schematic figure of the set up of the three moorings deployed around the Drygalski Ice Tongue in Terra Nova Bay. The DITN has been deployed since December 2014 until present, the DITS between February 2017 and January 2020 and the DITD from February 2017 until present. The Long moorings DITN and DITN have three pairs for CTD (SBE37SMP/SBE37SM) and current meters (Aquadopp) and an sequence of 4 thermistors (SBE56). Floats are indicative, see Fig. A1 in Appendix A for full schematic mooring diagram.

Table 1. The accuracy of the Thermo-haline instruments based on their manuals. The accuracy of the salinity is not given directly as it is calculated with the conductivity and temperature and the accuracy has been determined by lab experiments (Sea-Bird Scientific, 2026b).

Instrument	Measurement range	Initial Accuracy
SBE37SM	−5 to +35 °C	0.002 °C
Aquadopp	−4 to +40 °C	0.1 °C
SBE56	−5 to +45 °C	0.002 °C
RCM9	−3.01 to +5.92 °C	0.05 °C
SBE37SM	0–7 S m ^{−1}	0.0003 S m ^{−1}
	0–42 PSU	0.003–0.01 PSU

from 2017). The accuracy of the instruments are shown in Table 1 for the temperature and salinity and Table 2 for the current velocity. Measurement uncertainty is represented as shaded bands in the figures and is based on the manufacturer-specified initial accuracy for each instrument and measured variable.

The Drygalski Ice Tongue North mooring (DITN) is located on the northern side of the Drygalski Ice Tongue

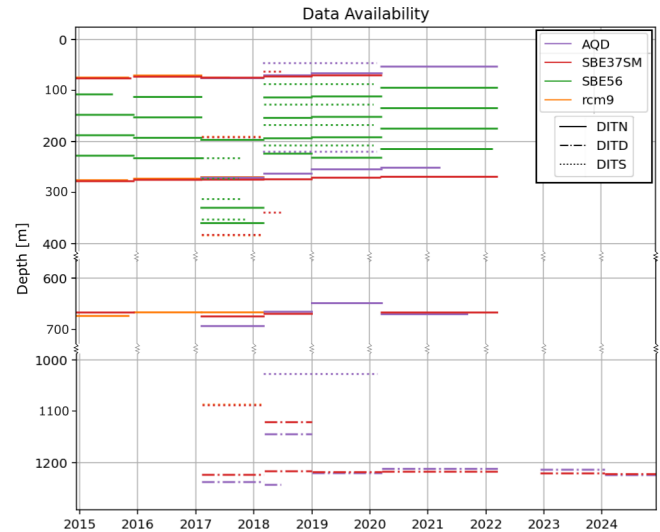


Figure 4. The data availability for each of the instruments at their corresponding depth based on the pressure measurements. The solid line are the instruments on the DITN, the dotted line on the DITD and the dot-dashed line on the DITS. The colors correspond with the instrument type, purple for the Aquadopp, red for the ctd SBE37SM(P), green for the thermistor SBE56 and orange for the current meter RCM9.

close to the ice tongue and was first deployed in December 2014. The bottom anchor sits at ~ 690 m depth. The DITN contains 4 groups of instruments, at the sub-surface at ~ 75 m depth a MicroCAT SBE37SM and an Aquadopp/RCM9, between 115–235 m depth. 4 SBE 56 thermistors, each 40 m vertical meters apart, a MicroCAT SBE37SM and Aquadopp/RCM9 at ~ 275 m depth and a MicroCAT SBE37 and Aquadopp/RCM9 close to the bottom at ~ 670 m depth. The RCM9 was used on the moorings: 1412DITN, 1512DITN and 1702DITN, the Aquadopp was first used on mooring 1702DITN, 1702DITD and 1702DITS and all future moorings.

The Drygalski Ice Tongue Deep mooring (DITD) is located slightly north-west of the DITN, in the Drygalski Basin anchored at ~ 1250 m depth. This mooring is equipped with 2 instruments near the bottom, a MicroCAT SBE37 and an Aquadopp at around 1240 m depth. In 2018, there were 2 mooring groups, both containing a MicroCAT SBE37 and an Aquadopp, at ~ 1140 and ~ 1240 m depth.

The Drygalski Ice Tongue South mooring (DITS) was deployed on the southern side of the Drygalski Ice Tongue between February 2017 until January 2020. In the first deployment year between February 2017 and March 2018, it was equipped with a MicroCAT SBE37SM and an RCM9 at ~ 190 m depth, 4 thermistors between 230 and 250 m each 40 m apart, a MicroCAT SBE37SM and an RCM9 at ~ 400 m depth and a MicroCAT SBE37SM and an RCM9 at ~ 1100 m depth. The second deployment was equipped with three MicroCAT SBE37SM and an Aquadopp pairs at ~ 48 m depth,

Table 2. The accuracy of the hydrodynamic instruments based on their manuals. The accuracy of the salinity is not given directly as it is calculated with the conductivity and temperature.

Instrument	Velocity range	Initial Accuracy	Magnetic resolution
Aquadopp	$\pm 100 \text{ cm s}^{-1}$, $\pm 250 \text{ cm s}^{-1}$, $\pm 500 \text{ cm s}^{-1}$	$\pm 1 \%$ of measured value $\pm 0.5 \text{ cm s}^{-1}$	2° for tilt $< 30^\circ$
RCM9	0 to 300 cm s^{-1}	0.3 cm s^{-1}	5° for $0\text{--}15^\circ$ tilt

at $\sim 230 \text{ m}$ depth and at $\sim 1050 \text{ m}$ depth and 4 thermistors between 90 and 210 m, spaced 40 m apart.

Each mooring was retrieved and redeployed every 1 to 2 years on a voyage, where the data is downloaded and instruments are serviced, battered, checked and calibrated before being deployed again. The MicroCAT SBE37SM(P) measures temperature, salinity (through conductivity) and pressure, the Aquadopp measures temperature, pressure, the direction and speed of the current and heading, pitch and roll, the SBE56 measures the temperature and RCM9 measures the speed and direction of the current. The depth averages described here is the mean depth derived from the pressure. The depth in each file in SEANOE is the mean depth derived from the pressure during that deployment. Outliers from mooring motions did not affect the mean significantly as the mean and median taken from the time-varying pressure are within the same depth in m.

Quality control

A number of checks are carried out to provide some assurance on data quality. The data collected by the instruments of the moorings are combined into netcdf files for each of the moorings per instrument type and deployment year. An overview of the available data is summarized in Tables 3, 4 and 5. The data is also checked on faulty and missing data, which are described in the corresponding section in Sect. 3. In some cases, the instruments started the measurement timeseries whilst still on the ship, this resulted in $+20^\circ$ temperatures, and pressure measurements at sea level. This data is removed in before the data processing.

The SBE37SM(P) instruments are calibrated before deployment by the CSIRO Oceanographic Calibration Facility to a factory calibration. The salinity is calculated through the conductivity and temperature. The accuracy of the salinity measurements have been examined by Uchida et al. (2008). The initial accuracy is found to be 0.003 PSU, or in TNB 0.0030 g kg^{-1} . Across different CTD instruments from Seabird, during long-term deployments (> 1 year) accuracy drifts to 0.01 PSU ($0.01008 \text{ g kg}^{-1}$ in TNB) in regions of strong temperature gradients (Wong et al., 2023). These uncertainties are below the range of seasonal and interannual variability and the instrument errors are solely in the range of the winter conditions and these instruments are very stable (Sea-Bird Scientific, 2010). The variability during winter is still valuable information as the instrument errors are

a shift, rather than noise. In addition to the factory calibration, a full-depth CTD cast was conducted right after each mooring deployment and again prior to recovery to use for the instrument drift calibration. The CTD profiles were obtained within a few hundred meters of the mooring location, as close to the mooring site as the environmental condition allowed, with a safety buffer to avoid entanglement with the mooring lines. The salinity measurements of the moored SBE37SM(P) instruments are post-calibrated with the profile measurements using the depth of the moored instruments.

$$\Delta S_{t_1} = S_{\text{CTD}_{\text{dep}}} - S_{\text{mooring}_{t_1}} \quad (1)$$

$$\Delta S_{t_f} = S_{\text{CTD}_{\text{rec}}} - S_{\text{mooring}_{t_f}} \quad (2)$$

$$S(t)_{\text{calibrated}} = S(t)_{\text{mooring}} + \Delta S_{t_1} + \frac{\Delta S_{t_f} - \Delta S_{t_1}}{N} \cdot t, \quad (3)$$

where $S_{\text{CTD}_{\text{dep}}}$ is the salinity measured by the CTD at depth of the instrument close to the time of deployment, $S_{\text{CTD}_{\text{rec}}}$ is the salinity measured by the CTD at depth of the instrument close to the time of recovery of the mooring, $S_{\text{mooring}_{t_1}}$ is the salinity measured by the mooring just after it is deployed, $S_{\text{mooring}_{t_f}}$ is the salinity measured by the mooring just before it is recovered and N is the number of observations made by the mooring. The mooring timeseries is only calibrated if ΔS_{t_1} or ΔS_{t_f} is larger than 0.003 PSU. This value is chosen as it is the lower bound of the uncertainties within SBE37SM(P) CTD instruments. In case that the instrument stopped recording before recovery, the calibration is done by $S(t)_{\text{calibrated}} = S(t)_{\text{mooring}} + \Delta S_{t_1}$. The temperature sensors were not adjusted post-deployment. Sea-Bird temperature sensors are highly stable and exhibit substantially lower drift than salinity, which is derived from conductivity and temperature. Applying a post-deployment temperature calibration to the SBE37SM(P) and SBE56 instruments would therefore likely introduce additional noise rather than improve data quality (Sea-Bird Scientific, 2010).

3 Oceanographic data

This section lists all the available data measured by the instruments on the DITx moorings in Terra Nova Bay. The mooring is referred to as [mooring][deployment year][deployment month], for example DITN1412. Details about the measurements are described per variable in the corresponding subsections, including the depth and period

Table 3. The meta-information about each mooring deployment and each installed sensors for DITN.

Instrument	Location	Depth [m]	Type	sn	start [dd/mm/yyyy]	end [dd/mm/yyyy]	interval [s]	data quality		
DITN – 1412	75°21.612' S, 164°44.971' E	75	RCM9	647	12/12/2014	20/11/2015	1800	No <i>T</i> data,		
		77	SBE37SM	5675	12/12/2014	20/11/2015	600			
		108	SBE56	2086	12/12/2014	27/07/2015	30			
		148	SBE56	2088	12/12/2014	10/12/2015	30			
		188	SBE56	2089	12/12/2014	10/12/2015	30			
		228	SBE56	2090	12/12/2014	10/12/2015	30			
		276	RCM9	845	12/12/2014	30/10/2015	1800			
		278	SBE37SM	7284	12/12/2014	10/12/2015	600			
		667	SBE37SM	5838	12/12/2014	10/12/2015	600			
		674	RCM9	847	12/12/2014	06/11/2015	1800	No <i>T</i> data,		
DITN – 1512	75°21.605' S, 164°44.918' E	71	RCM9	647	14/12/2015	08/02/2017	3600	<i>T</i> data faulty, removed		
		73	SBE37SM	5675	14/12/2015	08/02/2017	600			
		113	SBE56	5487	14/12/2015	08/02/2017	30			
		153	SBE56	2088	14/12/2015	08/02/2017	30			
		193	SBE56	2089	14/12/2015	08/02/2017	3S			
		233	SBE56	2090	14/12/2015	08/02/2017	30			
		273	RCM9	845	14/12/2015	08/02/2017	3600			
				275	SBE37SM	7284	14/12/2015		08/02/2017	600
				666	SBE37SM	5838	14/12/2015		08/02/2017	600
		667	RCM9	847	14/12/2015	08/02/2017	3600	No <i>T</i> data		
DITN – 1702	75°21.646' S 164°44.788' E	75	RCM9	1256	09/02/2017	01/08/2017	3600			
		75	SBE37SM	15 239	09/02/2017	06/03/2018	120			
		76	AQD	13 050	09/02/2017	06/03/2018	900			
		197	SBE56	4673	09/02/2017	06/03/2018	10			
		270	RCM9	1259	09/02/2017	06/03/2018	3600			
		271	AQD	9929	09/02/2017	06/03/2018	900			
		275	SBE37SM	15 240	09/02/2017	06/03/2018	120			
		330	SBE56	4852	09/02/2017	06/03/2018	10			
		360	SBE56	4854	09/02/2017	06/03/2018	10			
		667	RCM9	342	09/02/2017	06/03/2018	3600			
		675	SBE37SM	15 257	09/02/2017	06/03/2018	120			
		694	AQD	9930	09/02/2017	06/03/2018	900			

where observations are absent or need to be treated with caution due to faulty instruments or depleted batteries. The observational daily multi-year means are shown for the salinity, temperature, density and speed for the DITN and DITD mooring. The multi-year means are not shown for the observations of DITS as this mooring was only maintained for 3 years, with instruments at varying depths.

3.1 CTD results

Pressure is recorded by the Aquadopp and the MicroCAT, SBEs; the measurements per depth are plotted in Fig. 5 (DITN: panels a–c, DITS: panels d–f, DITD: panel g). The depth at which the variables are measured, as described in Tables 3, 4 and 5, are the mean values of the pressure-derived depth values. This mean is calculated by the median of the pressure derived depth values, to account for the mooring deflection due to strong wind-induced currents. The mean depth for instruments that do not record the pressure is cal-

culated based on linear interpolation and spacing between two known depths – i.e. between the bed anchor, and an SBE37SM(P). The instrument depths vary between deployments, so combining the datasets requires caution to account for differences in measurement levels.

The pressure derived depth also varies between deployments, as the depth varies, in the order of a few meters, due to the exact location of the mooring anchor, therefore the depth of the mooring anchor changes slightly each time the mooring is retrieved and deployed again. The pressure data shows bigger spikes in the instruments closer to the surface compared to the instruments closer to the bottom. These spikes are not removed from the data as they are caused by an increase in depth when the mooring line gets pulled down due to drag imposed by currents. This has no significant impact on the mean and median of the pressure derived depth, as they are short lived (order of hours) events.

Table 3. Continued.

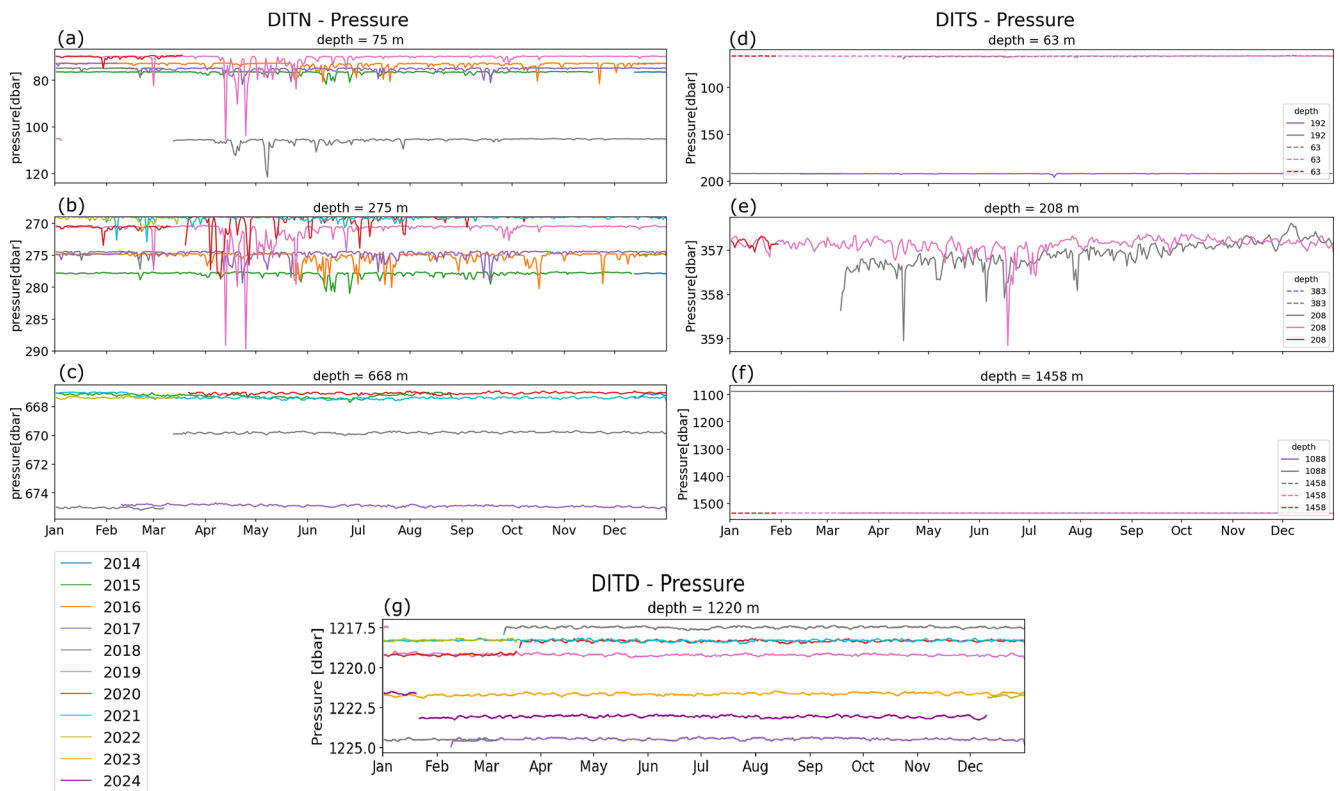
Instrument	Location	Depth [m]	Type	sn	start	end	interval [s]	data quality
DITN – 1803	75°21.660' S, 164°44.581' E	71	AQD	9929	12/03/2018	04/01/2019	600	
		73	SBE37SM	16 537	12/03/2018	04/01/2019	300	
		114	SBE56	4855	12/03/2018	04/01/2019	20	
		154	SBE56	4856	12/03/2018	04/01/2019	20	
		194	SBE56	6464	12/03/2018	04/01/2019	20	
		224	SBE56	8011	12/03/2018	04/01/2019	20	
		263	AQD	14 283	12/03/2018	04/01/2019	600	
		274	SBE37SM	16 566	12/03/2018	04/01/2019	300	
		666	AQD	14 372	12/03/2018	04/01/2019	600	
		670	SBE37SM	16 568	12/03/2018	04/01/2019	300	
DITN – 1901	75°20.914' S, 164°48.951' E	67	AQD	9929	04/01/2019	10/09/2019	600	
		71	SBE37SM	3431	07/01/2019	13/03/2020	300	
		112	SBE56	2098	07/01/2019	17/03/2020	30	
		152	SBE56	2115	07/01/2019	17/03/2020	30	
		192	SBE56	4851	07/01/2019	17/03/2020	30	
		232	SBE56	4857	07/01/2019	17/03/2020	30	
		255	AQD	14 283	04/01/2019	17/03/2020	600	
		271	SBE37SM	2443	07/01/2019	10/03/2020	120	
		649	AQD	14 372	04/01/2019	08/09/2019	600	
		647	SBE37SM	2444	–	–	–	Faulty data – removed
DITN – 2003	75°20.958' S, 164°49.021' E	53	SBE37SM	2444	–	–	–	Instrument flooded – no data
		54	AQD	14 292	18/03/2020	22/07/2020	600	
		95	SBE56	4855	18/03/2020	15/03/2022	60	
		135	SBE56	4856	18/03/2020	15/03/2022	60	
		175	SBE56	6464	18/03/2020	15/03/2022	60	
		215	SBE56	8011	18/03/2020	12/02/2022	60	
		269	SBE37SM	16 413	18/03/2020	15/03/2022	300	No S data
		252	AQD	14 289	18/03/2020	14/08/2020	600	
		667	SBE37SM	16 417	18/03/2020	15/03/2022	300	
		671	AQD	14 288	18/03/2020	24/08/2020	600	

Table 4. The meta-information about each mooring deployment and each installed sensors for DITD.

Instrument	Location	Depth [m]	Type	sn	start	end	interval [s]	data quality
DITD – 1702	75°16.542' S, 164°04.038' E	1225	SBE37SM	15 273	08/02/2017	06/03/2018	120	
		1239	AQD	13 041	08/02/2017	06/03/2018	900	
DITD – 1803	75°16.640' S, 164°04.260' E	1122	SBE37SM	15 273	10/03/2018	03/01/2019	60	
		1145	AQD	9930	10/03/2018	03/01/2019	600	
		1218	SBE37SM	15 242	10/03/2018	03/01/2019	180	
		1244	AQD	6162	10/03/2018	22/06/2018	600	
DITD – 1901	75°16.597' S, 164°04.198' E	1219	SBE37SM	4840	06/01/2019	17/03/2020	120	
		1221	AQD	9930	03/01/2019	12/03/2020	600	
DITD – 2003	75°16.681' S, 164°03.616' E	1213	AQD	14 383	18/03/2020	01/08/2020	600	
		1218	SBE37SM	15 273	18/03/2020	17/03/2022	300	
DITD – 2211	75°16.667' S, 164°3.642' E	1204	AQD	14 383	10/12/2022	21/01/2024	600	
		1205	SBE37SM	20 388	10/12/2022	21/01/2024	300	
DITD – 2401	75°16.660' S, 164°3.610' E	1206	SBE37SM	16 419	21/01/2024	08/12/2024	300	
		1214	AQD	9929	21/01/2024	08/12/2024	600	

Table 5. The meta-information about each mooring deployment and each installed sensors for DITS.

Instrument	Location	Depth [m]	Type	sn	start	end	interval [s]	data quality
DITS – 1702	75°29.305' S, 163°10.461' E	191	RCM9	647	12/02/2017	08/03/2018	3600	faulty <i>P</i> & <i>S</i> data removed
		192	SBE37SM	7227	12/02/2017	08/03/2018	300	
		233	SBE56	4855	12/02/2017	24/10/2017	10	
		273	SBE56	4856	12/02/2017	02/10/2017	10	
		313	SBE56	4857	12/02/2017	21/10/2017	10	
		353	SBE56	6464	12/02/2017	10/11/2017	10	
		383	SBE37SM	1627	12/02/2017	08/03/2018	300	
		384	RCM9	845	12/02/2017	08/03/2018	3600	
		1087	RCM9	847	12/02/2017	08/03/2018	3600	
1088	SBE37SM	7284	12/02/2017	08/03/2018	600			
DITS – 1803	75°29.313' S, 163°12.251' E	47	AQD	14 288	04/03/2018	28/02/2020	600	
		63	SBE37SM	15 239	10/03/2018	14/06/2018	20	
		88	SBE56	4673	09/03/2018	28/01/2020	20	
		128	SBE56	2089	09/03/2018	28/01/2020	20	
		168	SBE56	4852	09/03/2018	28/01/2020	20	
		208	SBE56	4854	09/03/2018	28/01/2020	20	
		220	AQD	14 289	04/03/2018	28/01/2020	600	
		339	SBE37SM	15 240	10/03/2018	18/06/2018	20	
		1027	AQD	14 290	04/03/2018	28/01/2020	600	
		1458	SBE37SM	15 257	10/03/2018	18/06/2018	20	

**Figure 5.** The pressure measured by the (a–c) DITN at ~75, ~275 and ~668 m depth, (d–f) by the DITS at ~48, ~192, ~220, ~1027 and ~1088 m depth and (g) by the DITD ~1220 m depth.

All SBE37SM(P), SBE56 and Aquadopp instruments measure the temperature. The depths of these instruments per mooring can be found in Tables 3, 4 and 5. Figure 6 shows the temperatures for each of the instruments (DITN: panels a–c, DITS: panels d–f, DITD: panel g). The accuracy of the Sea-Bird instrument are significantly better ($0.002\text{ }^{\circ}\text{C}$) than the Aquadopp ($0.01\text{ }^{\circ}\text{C}$) and the RCM9 ($0.05\text{ }^{\circ}\text{C}$) as shown in Table 1. Neither the SBEs, Aquadopp or RCM9 temperature sensors are calibrated as described in Sect. “Quality control”.

The temperatures measured in the top 400 m, show a clear seasonal signal, decreasing with depth, as shown in Fig. 6a, b, d and e. The temperature measured by the DITN near the surface at $\sim 75\text{ m}$ depth (Fig. 6a) increases from November, peaking at the end of February, it decreases during the Autumn months from March until June and during the winter months, the temperatures are $\sim -1.9\text{ }^{\circ}\text{C}$ and show the smallest variability at this mooring. In the Geiki inlet where the DITS is located, the temperature in the top 100 m (Fig. 6d) increases from the end of December, peak in February, and decreases until April where temperatures show low variability throughout the winter and spring. At 275 m depth at the DITN (Fig. 6b) and at 208 m at the DITS site (Fig. 6e), the temperature does not increase until late February. During April the highest temperatures of ~ -1.2 to $-1.7\text{ }^{\circ}\text{C}$ are recorded and they start to drop again during May and June. The winter period starts in July at the DITN site and in May at the DITS site with temperatures $\sim -1.9\text{ }^{\circ}\text{C}$ with super-cooled water reaching $< -2.0\text{ }^{\circ}\text{C}$. Near the bottom (Fig. 6c, g) temperatures range between -1.87 and $-1.91\text{ }^{\circ}\text{C}$, there is a decrease between July and November at the DITD and DITN locations and no clear seasonal signal at the DITS site (Fig. 6f). There is a strong temperature increase between end of April and start of May measured by the SBE37SM DITS1803_15239 at 63 m depth (Fig. 6d) and the SBE56 thermistor DITS1803_4854 at 208 m depth (Fig. 6e). Because this signal is measured two different instruments at two different depths, it is not removed from the final dataset, but should be treated with caution. Sudden large temperature changes (spikes) that last longer than 1 h are not removed from the dataset as the polynya is a highly active environment and sudden temperature changes can occur.

The temperatures are measured correctly for most of the instruments and moorings. The measurements that need to be treated with caution, are absent, or ignored due to faulty instruments are presented in Tables 3, 4 and 5. Aquadopp c1901DITN_9929 at 71 m depth (Fig. 6a) shows a sudden jump in temperature on 22 August 2019. At the same time as the sudden temperature increase, the pressure increases to 90 dbar at 15:30 NZST and decreases again to 68 dbar at 16:15 (Fig. 5a), while the temperature does not go back to the values before the sudden increase. This could indicate that the instrument got hit by an iceberg and possibly broke the temperature sensor. The temperature data after 22/8/2019T15:30 is removed in the final dataset.

The salinity is measured in PSU indirectly by the SBE37SM using conductivity and temperature, and converted to absolute salinity [g kg^{-1}] in this paper. At DITN near the surface at $\sim 75\text{ m}$ depth (Fig. 7a), the salinity decreases in the summer from the middle of January from 34.9 to 34.2 PSU. At $\sim 275\text{ m}$ depth (Fig. 7b), the salinity oscillates with the highest salinity in September and the lowest salinity in May. Close to the bottom, there is no obvious seasonal signal. In the Drygalski Basin, measured by the DITD (Fig. 7g), the salinity decreases slowly from the end of Autumn, with a sharp increase between September and October. The SBE37SM instruments on the DITS1803 mooring, measuring the salinity either did not record any data or stopped early. The salinity measurements are plotted in Fig. 7.

The in-situ density is measured for DITN at 75, 275 and 668 m depth, on DITD at 1220 m, on DITD1803 at 1120 m, on DITS1702 at 190, 390 and 1090 m, and on DITS1803 at 48, 240 and 1050 m. The MicroCAT did not record any density data from the DITN1902. Also there is no density data recorded on the DITN1512 mooring at 275 m (SBE37SM724) and 668 m (SBE37SM5838) depth. The missing density data can be calculated using the TEOS10 function with the salinity, temperature and pressure. The measured in-situ density on the DITN1902 mooring at 668 m depth, is faulty, as it is calculated with the salinity and temperature, which was not recorded correctly. The same applies to the DITS1803 mooring data at 48 and 240 m depth.

Water masses

We observe the following water masses in Terra Nova Bay near the Drygalski Ice Tongue: High Salinity Shelf Water (HSSW), defined as $\rho > 1028.00\text{ kg m}^{-3}$, Terra Nova Bay ice shelf water (TISW) where the temperature is below the surface freezing temperature $\text{CT} < \sim -1.94\text{ }^{\circ}\text{C}$ depending on salinity, and Antarctic Surface Water (ASW) $\text{CT} > -1.7\text{ }^{\circ}\text{C}$ (Yoon et al., 2020; Friedrichs et al., 2022). The TS-diagrams for the three depths that measure salinity in DITN and at DITD are shown in Fig. 8a–l and m–p respectively. The variability of the top half of the water column, up to 275 m depth (Fig. 8a–h), is forced by surface processes. The temperature and salinity response in the mid water-column (Fig. 8e–h) is shifted forward in time compared to the subsurface; in spring, we first observe a freshening and increase in temperature at 75 m depth (Fig. 8d), while fresher and warmer water masses don't reach deeper within the water column at 275 m depth (Fig. 8e) until summer. In Autumn, the subsurface (Fig. 8b) also cools and increases in salinity before the mid water column (Fig. 8f, g). The mixed layer depth rapidly increases between March and May and is assumed to be homogeneously mixed throughout the winter mass (Yoon et al., 2020), when HSSW is formed through sea ice formation during katabatic wind events. However, the HSSW formed in the eastern Terra Nova Bay does not convect all the way to the bottom, as the salinity observed in the top half of the water

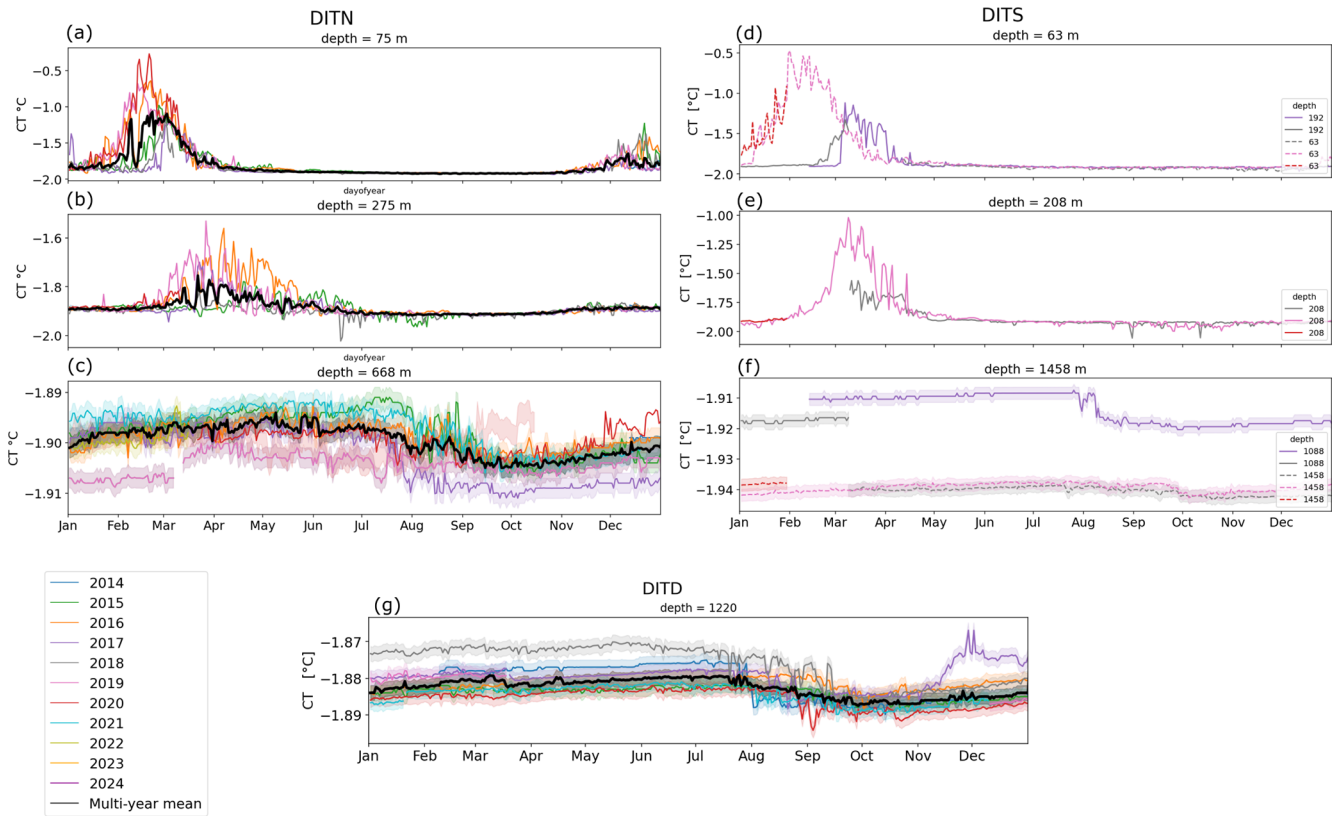


Figure 6. The temperature measured (a–c) by the DITN at ~ 75 , ~ 275 and ~ 668 m depth, (d–f) by the DITS at ~ 48 , ~ 63 , ~ 88 – 192 , ~ 208 , ~ 228 , ~ 383 , ~ 1064 , ~ 1088 and ~ 1458 m depth and (g) by the DITD ~ 1220 m depth. The observational multi-year mean is represented by the black line for DITN and DITD. DITS does not have enough observations to compute a multi-year mean. The calibration error and sensor drift are represented in the as uncertainty bands, based on the uncertainty of the corresponding instrument.

column (Figs. 7a, b and 8a, h) is fresher than observed at the bottom instrument of DITN (Figs. 7c and 8i–l) and the annual salinity increase is observed much later, between September and October, compared to the top half of the water column, as shown in Fig. 7a, b, d and e. Yoon et al. (2020) found a cyclonic circulation between 400–700 m depth in CTD and mooring observations (DITN, DITD and Mooring D) that advects HSSW, formed in front of the Nansen Ice Shelf, to the bottom instrument of DITN and the Drygalski Basin.

TISW is observed by DITN in the top half of the water column, where the Drygalski Ice Tongue extends to ~ 200 – 400 m depth. In the subsurface at 75 m depth (Figs. 6a and 8a–d), TISW is observed during winter and spring (Fig. 8c, d), while at 275 m depth (Fig. 8e, f) it is observed between summer and autumn, but with large interannual variability. This is in contrast to the Terra Nova Bay wide CTD observations in Yoon et al. (2020) that observed TISW at 275 m depth, however, they did find that the presence of TISW was dependent on the observation period. DITN is located close to the DIT, and the TISW observed by this mooring likely originates from water masses mixed with basal melt water from the ice tongue. Further study is needed to confirm this, as Yoon et al. (2020) found that TISW formed under the

Nansen Ice Shelf is advected in a cyclonic circulation similar to the HSSW.

3.2 Current meter results

The speed and direction of the current is measured with the RCM9 and Aquadopp instruments. On the DITN at 74, 76, 265, 274, 670 & 672 m depth. The RCM9 was installed on the DITN1412 & DITN1512 mooring at 74, 274 & 272 m depth and DITN1702 mooring at 74, 274 & 342 m depth and the Aquadopp at 76, 265 & 670 m depth from the DITN1702 mooring onwards. The DITD measures the currents with the Aquadopp at 1240 m depth. The currents are measured on the DITS1702 at 190, 390 and 1090 m depth with the RCM9, and on the DITS1803 50, 230 and 1060 m depth with the Aquadopp.

Figure 9 shows the hourly means of the current speed for each of the moorings. The current direction is corrected for the magnetic declination at the position of the mooring.

The prevailing direction of the flow shows in Fig. 10 measured by DITN is westerly near the surface at ~ 75 m depth (Fig. 10a) and in the middle of the water column at ~ 275 m depth (Fig. 10b). At the bottom at a depth of 670 m (Fig.

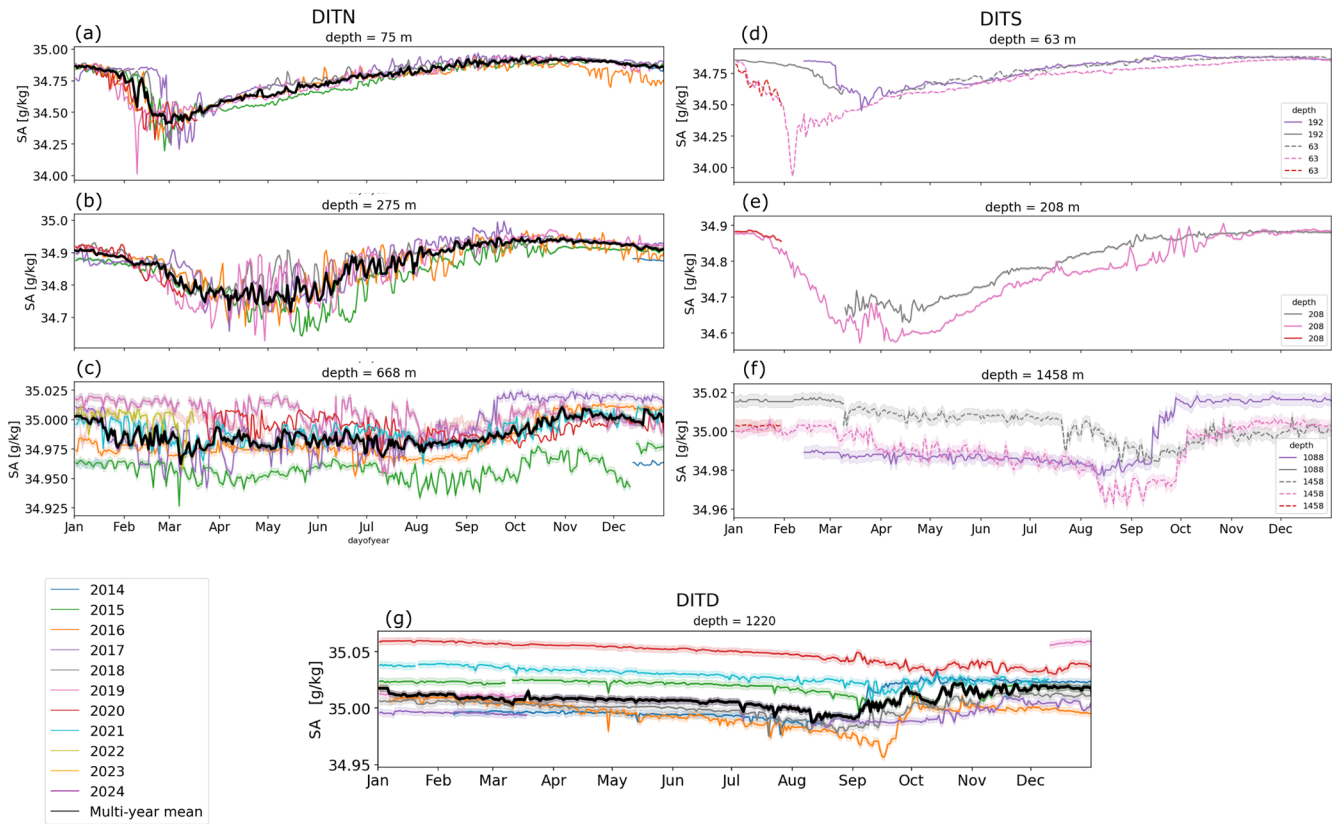


Figure 7. The salinity and 0.01 g kg^{-1} uncertainty measured (a–c) by the DITN at ~ 75 , ~ 275 and ~ 668 m depth, (d–f) by the DITS at ~ 63 , ~ 192 , ~ 208 , ~ 1088 and ~ 1458 m depth and (g) by the DITD ~ 1220 m depth. The observational multi-year mean is represented by the black line for DITN and DITD. DITS does not have enough observations to compute a multi-year mean. The calibration errors and sensor drift are represented in the as uncertainty bands, based on the uncertainty of the corresponding instrument.

10c), the current direction is very variable with a slight south westerly tendency. The flow at DITD (Fig. 10d) has a westward tendency, ranging between north west and south west or in north east direction. The bottom instrument of DITN and DITD show the largest variability, while the subsurface shows the smallest variability. This preferred westerly flow near the surface corresponds with the deflection of the Victoria Land Coastal current deflection observed in satellite data (Moctezuma-Flores et al., 2017).

The heading, roll and pitch are measured with the Aquadopp on the DITN1702 onwards at 76, 265 & 670 m depth, at 1145 & 1240 m on the DITD moorings and at 50, 230 and 1070 m on DITS1803. The heading is the rotation along the z -axis, the pitch along the x -axis and the roll along the y -axis. The heading, roll and pitch data can be used to study the movement of the mooring. The set-up, lengths between the instrument connections and length of the chains of the mooring can explain the variability in between mooring deployments.

3.3 Spectral analysis

A spectral analysis is performed to assess the dominant timescales of the observed velocities and pressure. The power spectral density (Fig. 11) shows two clear peaks at 1 and 2 cycles per day in the pressure data (Fig. 11e, f) in the bottom two instruments, corresponding to the diurnal and semi-diurnal tidal constituents, with the diurnal tide the dominant tidal frequency in the region. Near the surface (Fig. 11d) this signal is not as profound, suggesting the pressure is affected by other processes like surface gravity waves induced by wind that operate around the frequency of the tides. The spectral analysis of the speed data only shows a peak at one cycle per day (Fig. 11a) that corresponds with the tidal motion; at greater depth (Fig. 11b, c) these peaks are absent. The tidal constituents are not clearly visible in the speed data, likely because eddies are shed from the ice tongue and advected past the instruments, while the background currents driven by tidal motion move around the ice tongue. At greater depth, the diurnal and semi-diurnal tidal constituents are clearly evident in the pressure spectral analysis, reflecting the dominance of barotropic tidal forcing where surface effects and transient processes such as wind or ice interactions

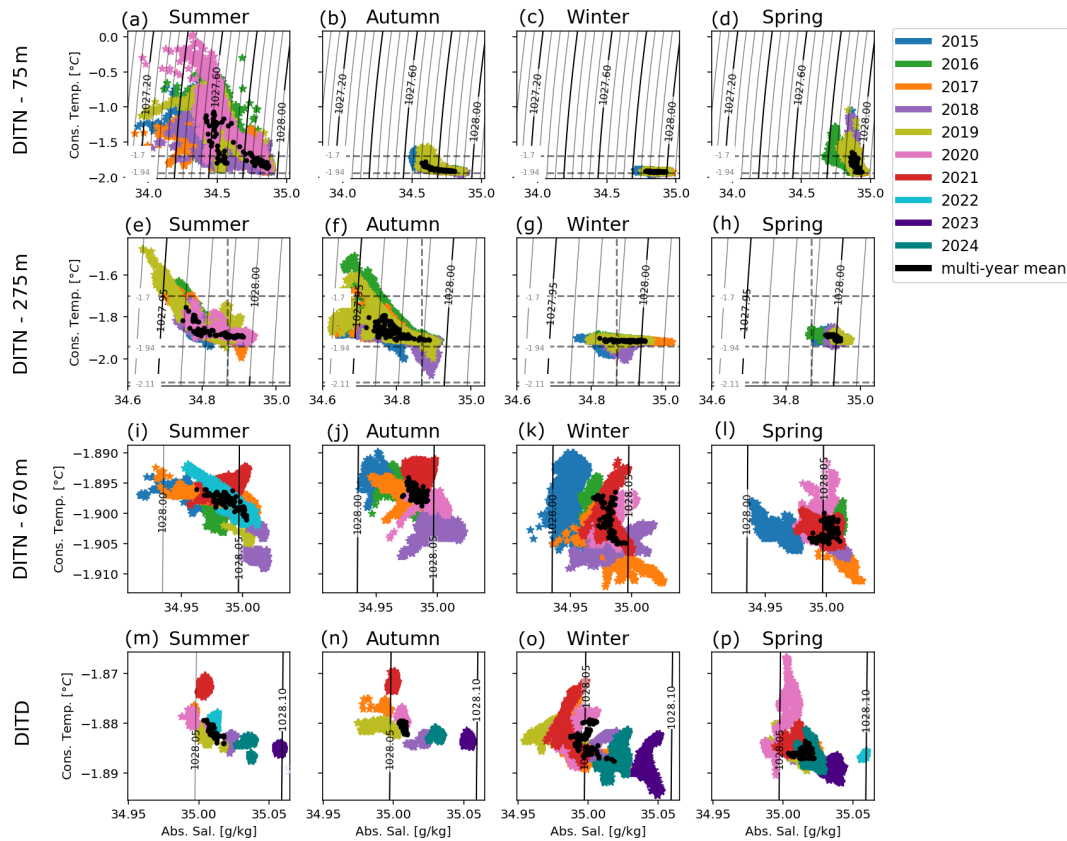


Figure 8. The absolute salinity versus the conserved temperature per season for each depth, colored by year. The daily multi-year mean over the observed years is plotted in black. Summer is defined as the period from 1 January until 1 April, Autumn from 1 April until 1 July, Winter from 1 July until 1 October and Spring from 1 October until 1 January. The isopycnals are plotted at 0.05 kg m^{-3} intervals, with inline values. The isotherms define the ISW ($CT < T_{f5}$) and AAWs ($CT > -1.7 \text{ [}^\circ\text{C]}$).

are minimal. A distinct secondary peak is observed near 0.2 cycles per day (Fig. 11a), indicating variability on a 3–5 d timescales. These lower scale fluctuations represent the inertial and sub-inertial variability like eddies and synoptic forcing like storms and katabatic wind events.

4 Code and data availability

This paper provides a detailed description of the temporal coverage of the dataset, which consists of a near-continuous high-temporal-resolution time series of currents, temperature, and salinity from December 2014 to December 2024. The methodology adopted for settings, data recording, and quality control ensures the dataset's compliance and consistency. Although the dataset currently ends in December 2024, monitoring activities are ongoing. Future data from this hydrographic timeseries will be added to an updated version of the repository as future moorings are recovered. All coding used to make the datafiles are uploaded to Zenodo: <https://doi.org/10.5281/zenodo.20376404> (Cornelissen, 2026). The data of the three hydrographic

moorings are uploaded as netcdf files to SEANOE in <https://doi.org/10.17882/102640> (Cornelissen et al., 2025).

5 Discussion and Conclusions

This paper shows the data collected by three mooring around the Drygalski Ice Tongue in Terra Nova Bay between December 2014 and December 2024. The Drygalski Ice Tongue is a prominent feature in Terra Nova Bay and blocks the inflow of sea ice from the south, enabling it to operate as a polynya during the colder months of the year. The water masses formed in Terra Nova Bay interact with the Drygalski Ice Tongue and variability in these water masses is relevant for understanding ocean conditions in its vicinity and broader ice-ocean interactions (Wang et al., 2023). Long-term observations provide important context for monitoring hydrographic variability close to the Drygalski Ice Tongue. As the Drygalski Ice Tongue also extends into the water column, it also affects the circulation and advection of water masses within Terra Nova Bay and the exchange below the ice tongue (Stevens et al., 2024). A modelling study that represented a polynya similar to Terra Nova Bay done by Xu et al. (2023), found that an ice

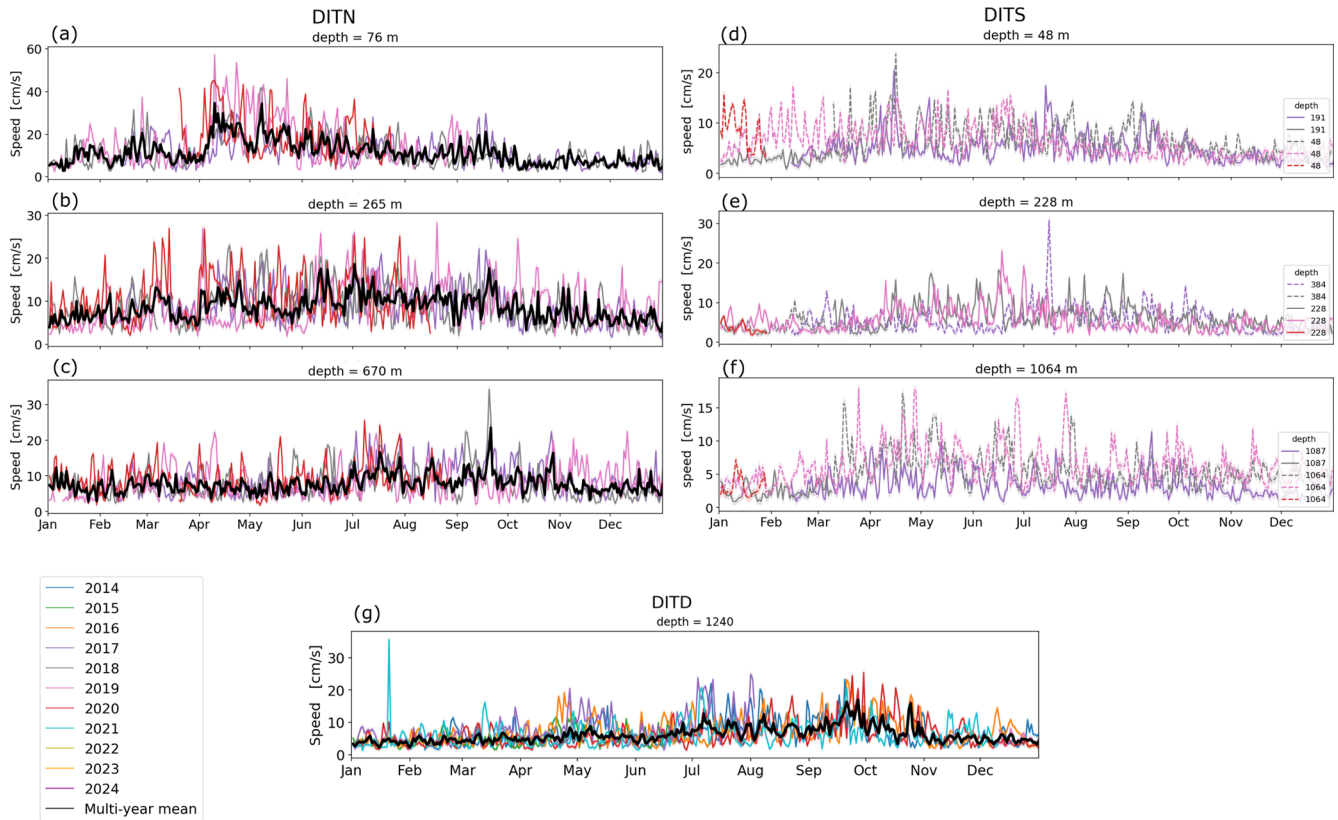


Figure 9. The current speed measured (a) by the DITN at ~ 76 , ~ 265 , and ~ 670 m depth, (b) by the DITS at ~ 48 , ~ 191 , ~ 228 , ~ 384 , ~ 1064 and ~ 1087 m depth and (c) by the DITD ~ 1240 m depth. The observational multi-year mean is represented by the black line for DITN and DITD. DITS does not have enough observations to compute a multi-year mean. The calibration errors and sensor drift are represented in the as uncertainty bands, based on the uncertainty of the corresponding instrument.

Current velocity per mooring at DITN & DITD

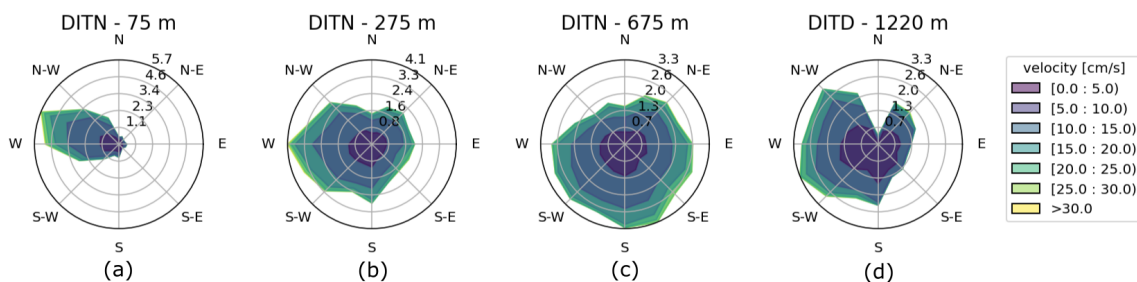


Figure 10. The currents measured by the three DITN aquadopps and the DITD are plotted per instrument. The contours represent the direction and speed of the currents of the total observed period. The radius of the bar represents the frequency of the occurrence.

tongue in a coastal polynya changes the circulation patterns compared to polynya that is not bound by an ice tongue. They observed a surface flow along the ice tongue towards the ice shelf front, which corresponds with the westerly flow observed at the subsurface instrument of DITN. Together, these observations provide in-situ context for interpreting seasonal and interannual variability of the circulation patterns close to the ice tongue.

Outlook and uses of data

The described hydrographic mooring time series, presented in this paper, is a valuable tool to increase our understanding of the highly dynamic polynya system. Comparing this data set with other observations in Terra Nova Bay, helps with the horizontal extent of the polynya dynamics and variability. The length of the observations closer to the surface, provides insight into the drivers of and interannual variability of

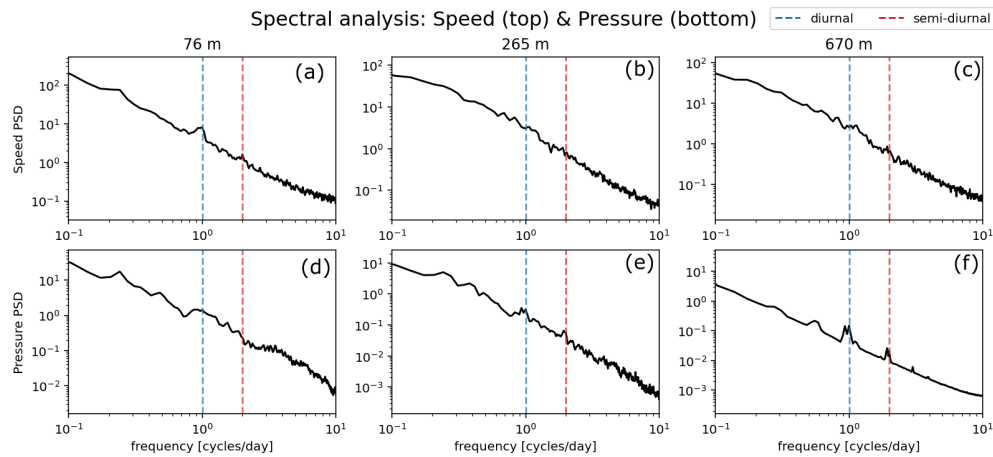


Figure 11. The spectral density analysis of the speed (top row) and pressure (bottom row) data of all years at the current meters at ~ 76 , ~ 265 and ~ 670 m depth. Vertical dashed lines indicate diurnal (blue) and semi-diurnal (red) tidal frequencies.

water mass formation processes. This long-term dataset constrains variability associated with atmospheric conditions, sea ice dynamics, and ocean circulation patterns, that influence the timing, amount, and properties of HSSW rather than allowing direct attribution and supports future investigation of how the Drygalski Ice Tongue itself may influence these processes. We aim to determine the origin of water masses observed near the Drygalski Ice Tongue during the winter months when HSSW is formed while bay-wide CTD observations are impossible. In future work we also aim to use idealised and regional models to complement the observational dataset.

The datasets from DITN and DITS are also valuable for biological applications. Both DITN and DITS include instruments located within the euphotic zone, allowing for the analysis of the mixed layer depth and its variability. Due to close proximity of DITN and DITS to the Drygalski Ice Tongue, these datasets offer an opportunity to investigate oceanographic conditions in the vicinity of the ice tongue that are relevant for understanding ice-ocean interaction, rather than assessing ice-tongue stability or evolution. These moorings can give an in-situ oceanographic perspective that complements changes observed with radar and satellite data. When combined with radar and satellite imagery, the in-situ data provide a complementary oceanographic perspective, enhancing our understanding of ice-ocean interactions and supporting interdisciplinary studies linking ocean physics, glaciology, and marine biology.

Appendix A: Additional figures

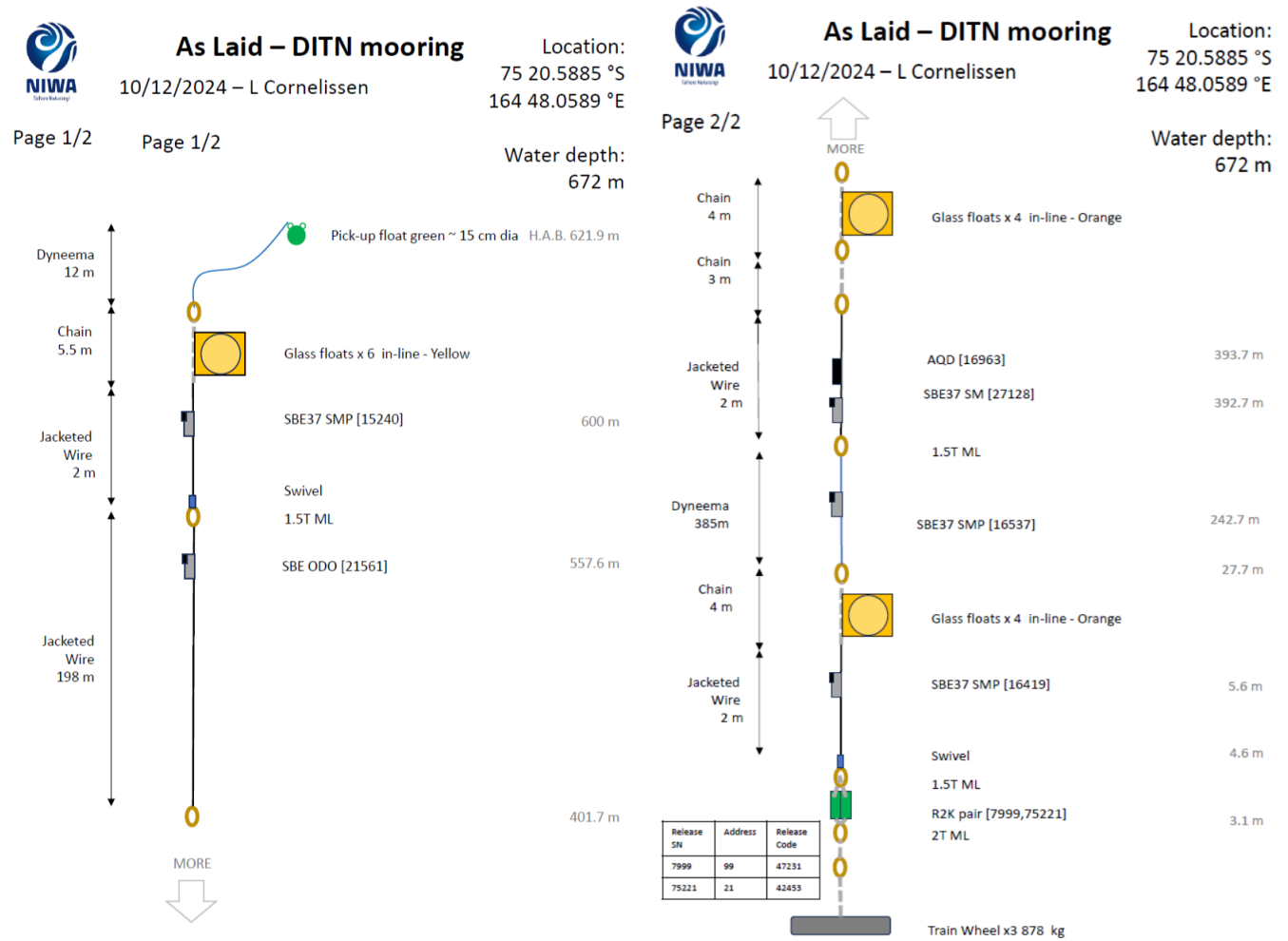


Figure A1. Mooring diagram of DITN for the December 2024 deployment, showing instrument specifications and serial numbers, as well as flotation and line details. Depths of instruments that do not record pressure are determined from their relative distance to instruments that do using these diagrams.

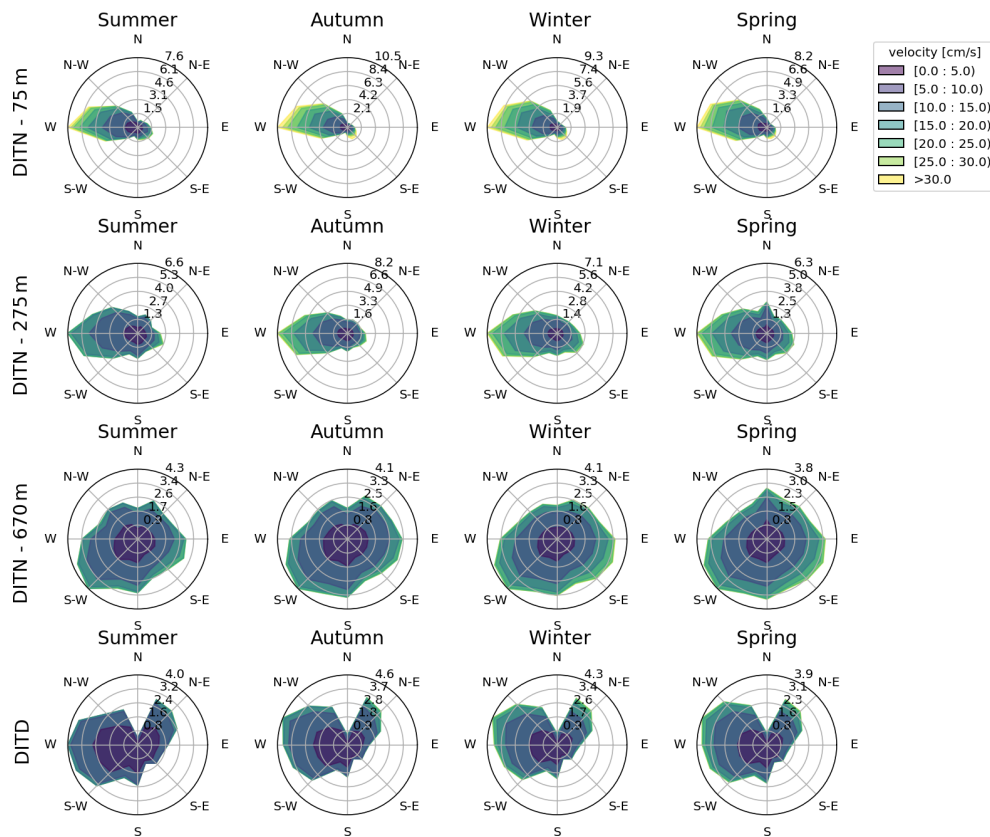


Figure A2. The currents measured by the three DITN aquadopps and the DITD are plotted per instrument, per season. The contours represent the direction and speed of the currents of the total observed period. The radius of the bar represents the frequency of the occurrence.

Author contributions. The dataset was assembled and checked by LC. The deployment and recovery of the moorings were led by JMc, BG, FE, CJZ, SY, STY and LC on various voyages with the assistance of the *Araon* and *Laura Bassi* deck crew. The timeseries was initiated by CS, WSL and CJZ. LC wrote up the manuscript and all other co-authors helped improve it.

Competing interests. The contact author has declared that none of the authors has any competing interests.

Disclaimer. Publisher's note: Copernicus Publications remains neutral with regard to jurisdictional claims made in the text, published maps, institutional affiliations, or any other geographical representation in this paper. The authors bear the ultimate responsibility for providing appropriate place names. Views expressed in the text are those of the authors and do not necessarily reflect the views of the publisher.

Acknowledgements. The authors wish to thank the Korea Polar Research Institute (KOPRI), the New Zealand Antarctic Research Institute, the N.Z. Antarctic Science Platform and Antarctica New Zealand for support. We especially thank the crew of the IBRV *Araon* and *Laura Bassi*. The mooring instruments are provided by the NIWA Capex Program. We thank Gary Wilson and Richard Levy for their support in initiating this work. In addition, we acknowledge Pierpaolo Falco and Pasquale Castagno who assisted in recovery of the DITS mooring with the *Laura Bassi*. SY and WSL are supported by the Korea Institute of Marine Science & Technology Promotion (KIMST) funded by the Ministry of Oceans and Fisheries (RS-2023-00256677; PM25020).

Financial support. This paper forms a contribution to Phase One (ANTA1801) and Phase Two (ANTARCTICANZ2504) of the New Zealand Antarctic Science Platform. This research has been supported by the Korea Institute of Marine Science and Technology promotion (grant nos. RS-2023-00256677 and PM25020), and the Office of Polar Programs (grant nos. 1341688 and 2332418). Support for C.J.Z. was provided by the NSF Office of Polar Programs (OPP) award 2332418. STY was supported by the Korea Institute of Marine Science & Technology Promotion (KIMST), funded by the Ministry of Oceans and Fisheries (RS-2023-00256677; PM25020), and by the Basic Science Research Program of the National Re-

search Foundation of Korea (NRF), funded by the Ministry of Science and ICT (RS-2025-19623001).

Review statement. This paper was edited by Guillaume Charria and reviewed by two anonymous referees.

References

- Argo: Argo Fleet Monitoring – Euro-Argo, <https://fleetmonitoring.euro-argo.eu/dashboard?Status=Active,Inactive&WMO=3902666,5907101,6903812,6903795> (last access: 9 January 2026), 2000.
- Bianchi, N. C., Chiappini, N. M., Tabacco, N. I. E., Passerini, N. A., Zirizzotti, N. A., and Zuccheretti, N. E.: Morphology of bottom surfaces of glacier ice tongues in the East Antarctic region, *Ann. Geophys.*, 44, <https://doi.org/10.4401/ag-3609>, 2001.
- Castagno, P., Capozzi, V., DiTullio, G. R., Falco, P., Fusco, G., Rintoul, S. R., Spezie, G., and Budillon, G.: Rebound of shelf water salinity in the Ross Sea, *Nat. Commun.*, 10, <https://doi.org/10.1038/s41467-019-13083-8>, 2019.
- Cornelissen, L.: Livcornelissen/DIT_mooringdata: Processing and Quality Control Code for DIT Mooring Data (v1.0), Zenodo [code], <https://doi.org/10.5281/zenodo.20376404>, 2026.
- Cornelissen, L., Yun, S., McInerney, J., Grant, B., Elliot, F., Yoon, S., Zappa, C. J., Lee, W. S., and Stevens, C.: A decade-long hydrographic mooring dataset near the Drygalski Ice Tongue, Terra Nova Bay, Antarctica, SEANOE [data set], <https://doi.org/10.17882/102640>, 2025.
- Frezzotti, M. and Mabin, M.: 20th century behaviour of Drygalski Ice Tongue, Ross Sea, Antarctica, *Ann. Glaciol.*, 20, 397–400, <https://doi.org/10.3189/172756494794587492>, 1994.
- Friedrichs, D. M., McInerney, J. B. T., Oldroyd, H. J., Lee, W. S., Yun, S., Yoon, S., Stevens, C. L., Zappa, C. J., Dow, C. F., Mueller, D., Steiner, O. S., and Forrest, A. L.: Observations of submesoscale eddy-driven heat transport at an ice shelf calving front, *Commun. Earth Environ.*, 3, <https://doi.org/10.1038/s43247-022-00460-3>, 2022.
- Gomez-Fell, R., Marsh, O. J., Rack, W., Wild, C. T., and Purdie, H.: Basal mass balance and prevalence of ice tongues in the Western Ross Sea, *Front. Earth Sci.*, 11, <https://doi.org/10.3389/feart.2023.1057761>, 2023.
- Gossart, A., Malyarenko, A., Cornelissen, L., Stevens, C., Miller, U., Zappa, C. J., Luca, N., Castagno, P., and Budillon, G.: Representation of polynyas in the Ross Sea coupled atmosphere–sea ice–ocean model P-SKRIPsv2, EGU sphere [preprint], <https://doi.org/10.5194/egusphere-2025-4332>, 2025.
- Haran, T., Klinger, M., Bohlander, J., Fahnstocck, M., Painter, T., and Scambos, T.: MEASUREs MODIS Mosaic of Antarctica 2013–2014 (MOA2014) Image Map, Version 1, NSIDC-0730, NASA National Snow and Ice Data Center Distributed Active Archive Center, Boulder, Colorado, USA [data set], <https://doi.org/10.5067/RNF17BP824UM>, 2018.
- Indrigo, C., Dow, C. F., Greenbaum, J. S., and Morlighem, M.: Drygalski Ice Tongue stability influenced by rift formation and ice morphology, *J. Glaciol.*, 67, 243–252, <https://doi.org/10.1017/jog.2020.9>, 2021.
- Malyarenko, A., Gossart, A., Sun, R., and Krapp, M.: Conservation of heat and mass in P-SKRIPsv2 version 1: the coupled atmosphere–ice–ocean model of the Ross Sea, *Geosci. Model Dev.*, 16, 3355–3373, <https://doi.org/10.5194/gmd-16-3355-2023>, 2023.
- Miller, U. K., Zappa, C. J., Gordon, A. L., Yoon, S., Stevens, C., and Lee, W. S.: High salinity shelf water production rates in Terra Nova Bay, Ross Sea, *Nat. Commun.*, 15, <https://doi.org/10.1038/s41467-023-43880-1>, 2024.
- Moctezuma-Flores, M., Parmiggiani, F., Fragiaco, C., and Guerrieri, L.: Synthetic aperture radar analysis of floating ice at Terra Nova Bay – an application to ice eddy parameter extraction, *J. Appl. Remote Sens.*, 11, <https://doi.org/10.1117/1.JRS.11.026041>, 2017.
- Morales Maqueda, M. A., Willmott, A. J., and Biggs, N. R. T.: Polynya dynamics: a review of observations and modeling, *Rev. Geophys.*, 42, RG1004, <https://doi.org/10.1029/2002RG000116>, 2004.
- Morlighem, M., Favier, L., Seroussi, H., Rignot, E., Larour, E., Ben Dhia, H., and Aubry, D.: BedMachine Antarctica v3, *Geophys. Res. Lett.*, 47, e2020GL088569, <https://doi.org/10.5067/FPSU0V1MWUB6>, 2020.
- MORSea: Marine Observatory in the Ross Sea, Italian National Antarctic Research Program (PNRA), coordinated by University of Naples “Parthenope” and CNR, <https://morsea.uniparthenope.it> (last access: 9 January 2026), 2009.
- Nicholls, K. W.: Predicted reduction in basal melt rates of an Antarctic ice shelf in a warmer climate, *Nature*, 388, 460–462, <https://doi.org/10.1038/41302>, 1997.
- Nortek: Norway, Aquadopp 6000M manual, <https://www.nortekgroup.com/products/aquadopp2-6000-m/pdf> (last access: 9 January 2026), 2026.
- Otago Sea Ice Monitoring Station: Antarctic Science Platform’s Sea Ice and Carbon Cycle Feedbacks Project, <https://seaice.otago.ac.nz/trackers/overview/> (last access: 9 January 2026), 2026.
- Rusciano, E., Budillon, G., Fusco, G., and Spezie, G.: Evidence of atmosphere–sea ice–ocean coupling in the Terra Nova Bay polynya, *Cont. Shelf Res.*, 61–62, 112–124, <https://doi.org/10.1016/j.csr.2013.04.002>, 2013.
- Sea-Bird Scientific: Sea-Bird Electronics, Application Note 31: Temperature and conductivity corrections (February 2010), <https://imos.org.au/wp-content/uploads/2024/07/appnote31Feb10TempandCondCorrections.pdf> (last access: 9 January 2026), 2010.
- Sea-Bird Scientific: SBE37SM/SBE37SMP, Bellevue, WA, USA, https://www.comm-tec.com/prods/mfsgs/SBE/manuals_pdf/SBE37SM_016.pdf (last access: 9 January 2026), 2026a.
- Sea-Bird Scientific: Frequently asked questions: CTD accuracy and effect of fouling/contamination on conductivity/salinity data, <https://blog.seabird.com/faqs/> (last access: 9 January 2026), 2026b.
- Sea-Bird Scientific: SBE56, Bellevue, WA, USA, https://www.comm-tec.com/Prods/mfsgs/SBE/brochures_pdf/56brochureApr11.pdf (last access: 9 January 2026), 2026c.
- Stevens, C., Lee, W. S., Fusco, G., Yun, S., Grant, B., Robinson, N., and Hwang, C. Y.: The influence of the Drygalski Ice Tongue on the local ocean, *Ann. Glaciol.*, 58, 51–59, <https://doi.org/10.1017/aog.2017.4>, 2017.

- Stevens, C., Yoon, S., Zappa, C. J., Miller, U. K., Wang, X., Elliott, F., Cornelissen, L., Lee, C., Yun, S., and Lee, W. S.: Ocean processes south of the Drygalski Ice Tongue, western Ross Sea, *Deep-Sea Res. Pt. II*, 217, 105411, <https://doi.org/10.1016/j.dsr2.2024.105411>, 2024.
- Tamura, T., Ohshima, K. I., Fraser, A. D., and Williams, G. D.: Sea ice production variability in Antarctic coastal polynyas, *J. Geophys. Res.-Oceans*, 121, 2967–2979, <https://doi.org/10.1002/2015JC011537>, 2016.
- Uchida, H., Kawano, T., and Fukasawa, M.: In situ calibration of moored CTDs used for monitoring abyssal water, *J. Atmos. Ocean. Technol.*, 25, 1695–1702, <https://doi.org/10.1175/2008jtecho581.1>, 2008.
- Wang, Y., Zhou, M., Zhang, Z., and Dinniman, M. S.: Seasonal variations in Circumpolar Deep Water intrusions into the Ross Sea continental shelf, *Front. Mar. Sci.*, 10, <https://doi.org/10.3389/fmars.2023.1020791>, 2023.
- Wong, A. P. S., Gilson, J., and Cabanes, C.: Argo salinity: bias and uncertainty evaluation, *Earth Syst. Sci. Data*, 15, 383–393, <https://doi.org/10.5194/essd-15-383-2023>, 2023.
- Yoon, S.-T., Lee, W. S., Stevens, C., Jendersie, S., Nam, S., Yun, S., Hwang, C. Y., Jang, G. I., and Lee, J.: Variability in high-salinity shelf water production in the Terra Nova Bay polynya, Antarctica, *Ocean Sci.*, 16, 373–388, <https://doi.org/10.5194/os-16-373-2020>, 2020.
- Xu, Y., Zhang, W., Maksym, T., Ji, R., and Li, Y.: Stratification breakdown in Antarctic coastal polynyas. Part II: influence of an ice tongue and coastline geometry, *J. Phys. Oceanogr.*, 53, 2069–2088, <https://doi.org/10.1175/jpo-d-22-0219.1>, 2023.
- Xylem Inc.: RCM9, Rye Brook, NY, USA, <https://epic.awi.de/id/eprint/45145/1/RCM9.pdf> (last access: 9 January 2026), 2026.